Journal of Biomolecular NMR **27:** 221–234, 2003.

^{15}N relaxation study of the cold shock protein CspB at various solvent viscosities

Markus Zeeb[a], Maik H. Jacob[a], Thomas Schindler[a,b] & Jochen Balbach[a,*]
[a]*Laboratorium für Biochemie, Universität Bayreuth, D-95440 Bayreuth, Germany*
[b]*Present address: Hoffmann LaRoche AG, CH-4070 Basel, Switzerland*

Received 10 February 2003; Accepted 2 June 2003

Key words: chemical exchange, correlation time, diffusion, dynamics, ethylene glycol, NMR relaxation, protein folding, viscosity

Abstract

For a detailed NMR study of the dynamics of the cold shock protein CspB from *Bacillus subtilis*, we determined ^{15}N transverse and longitudinal relaxation rates and heteronuclear nuclear Overhauser effects at different solvent viscosities. Up to a relative viscosity of 2, which is equivalent to 27% ethylene glycol (EG), the overall correlation time follows the linear Stokes-Einstein equation. At a relative viscosity of 6 (70% EG) the correlation time deviates from linearity by 30%, indicating that CspB tumbles at a higher rate as expected from the solvent viscosity probably due to a preferential binding of water molecules at the protein surface. The corresponding hydrodynamic radii, determined by NMR diffusion experiments, show no variation with viscosity. The amplitudes of intramolecular motions on a sub-nanosecond time scale revealed by an extended Lipari–Szabo analysis were mainly independent of the solvent viscosity. The lower limit of the NMR 'observation window' for the internal correlation time shifts above 0.5 ns at 70% EG, which is directly reflected in the experimentally derived internal correlation times. Chemical exchange contributions to the transverse relaxation rates derived from the Lipari-Szabo approach coincide with the experimentally determined values from the transverse ^{1}H-^{15}N dipolar/^{15}N chemical shift anisotropy relaxation interference. These contributions originate from fast protein folding reactions on a millisecond timescale, which get retarded at increased solvent viscosities.

Introduction

NMR spectroscopy covers a wide range of time regimes, which allows to observe phenomena in proteins from rapid motions on a picosecond time scale by relaxation studies (Palmer, 1997) up to H/D exchange (Bai et al., 1994) and protein folding reactions on a minute to hour time scale (van Nuland et al., 1998). For the interpretation of protein relaxation parameters in terms of motion, two formalisms are favored: the model-free approach (Lipari and Szabo, 1982a; Lipari and Szabo, 1982b) and spectral density mapping (Peng and Wagner, 1992). Typically, longitudinal spin-lattice relaxation (R_1), transverse spin-spin relaxation (R_2), and the heteronuclear NOE effect (*hNOE*) are determined for every heteronucleus (Palmer, 1997). Additional experimental relaxation data include longitudinal two-spin order, antiphase two-spin coherence, amide-proton in-phase coherence and amide-proton longitudinal magnetization (Dayie and Wagner, 1994). Experimental access to dynamic processes via CPMG and $R_{1\rho}$ relaxation techniques of proteins on microsecond-millisecond time scales has been realized more recently (Palmer et al., 2001). To increase the amount of experimental data for the calculation of parameters of motion, relaxation rates at different field strengths (Canet et al., 2001) and temperatures (Seewald et al., 2000) have to be acquired.

We followed an alternative approach to increase the number of experimental relaxation data by varying the solvent viscosity. The protein under investigation

*To whom correspondence should be addressed. E-mail: jochen.balbach@uni-bayreuth.de

is the cold shock protein CspB of *Bacillus subtilis*. Recent studies showed that both, unfolding and refolding of CspB are significantly decelerated when the viscosity of the solvent increases by adding ethylene glycol or sucrose (Jacob et al., 1997, 1999). Therefore we ask the question, whether a variation of the solvent viscosity can provide additional information for the interpretation of relaxation rates and of chemical exchange contributions to these rates from protein folding reactions.

To approach these questions, we determined overall rotational correlation times τ_m from ^{15}N-relaxation rates R_1, R_2 and heteronuclear NOEs at three different solvent viscosities employing an extended Lipari-Szabo formalism. We found a non-linear dependence of τ_m on the macroscopic viscosity but invariant hydrodynamic radii of CspB. Faster internal motions are mainly independent of the viscosity. The conformational exchange contributions R_{ex} to R_2 originating mainly from the folding/unfolding equilibrium have been determined experimentally from the interference between ^{1}H-^{15}N dipolar and ^{15}N chemical shift anisotropy (CSA) interactions. We found a good coincidence between these experimental R_{ex} rates and R_{ex} contributions determined by the extended Lipari-Szabo analysis. Reduced chemical exchange rates at higher viscosities arise from changes of the folding rates of CspB under these conditions.

Experimental procedures

^{15}N labeling and sample preparation

CspB from *Bacillus subtilis* was overexpressed in *Escherichia coli* BL21(DE3) pPDCSP using the bacteriophage T7 polymerase system under the control of the tac hybrid promotor. The bacteria were grown in M9 minimal medium (Sambrook et al., 1989) at 37 °C supplemented with $^{15}NH_4Cl$ and induced with 1 mM IPTG at $OD_{600} = 0.7$. The following purification was achieved as described previously (Schindler et al., 1995) after reaching an OD_{600} of 1.5. NMR samples for heteronuclear correlation experiments contained 1.5 mM ^{15}N-CspB, 7% D_2O in 100 mM Na-cacodylate/HCl at pH 7.0 with 0%, 27%, and 70% (w/v) ethylene glycol (EG). For diffusion experiments 1.0 mM unlabeled CspB was dissolved within the same buffer in D_2O and various amounts of deuterated ethylene glycol (d6-EG) containing 0.1% dioxan. Solvent viscosities of the respective EG solutions were measured with an oscillating capillary rheometer OCR-D from Chempro (Jacob et al., 1997).

NMR measurements

All spectra were acquired at 25 °C with a Bruker DRX500 or DRX600 spectrometer with 2048 complex points for 1D spectra and 1024 × 128 complex points for 2D spectra. PG-SLED gradient echo experiments (Gibbs and Johnson, 1991; Jones et al., 1997) were recorded at a ^{1}H resonance frequency of 500 MHz. For each set, 18 different gradient strengths were used for the 5.75 ms de- and refocusing gradient along the z-axis followed by a 2 ms recovery delay (Jones et al., 1997). Diffusion was allowed to proceed for 80 ms (0%, 27%) or 140 ms (52% EG, 70% EG) to ensure a protein signal intensity decay of 70% to 90% at the highest gradient strength. All other pulses and delays and the 1 ms spoil gradients before data acquisition were kept constant. Each measurement was repeated three times to improve signal-to-noise ratio and to estimate the errors. Equation 1 can be fitted to the NMR intensities *I(g)* at the respective gradient strength g (Balbach, 2000; Jones et al., 1997). *I(g)* is the integral typically between 0.5 ppm and 2.5 ppm. The translational diffusion coefficient of the protein is proportional to d_{prot} and A represents the amplitude of the Gaussian diffusion curve.

$$I(g) = A \cdot \exp(-d_{prot} \cdot g^2). \quad (1)$$

The reference integral of the dioxan resonance at 3.6 ppm contains small contributions from the protein. Therefore, d_{diox} was derived from Equation 2, with fixed d_{prot} and A_{prot} and A_{diox} representing the Gaussian contributions of the protein and dioxan, respectively.

$$I(g) = A_{diox} \cdot \exp(-d_{diox} \cdot g^2) + A_{prot} \cdot \exp(-d_{prot} \cdot g^2). \quad (2)$$

The hydrodynamic radius of the protein (R_H^{prot}) was calculated according to Equation 3 using a reference radius for dioxan (R_H^{diox}) of 2.12 Å (Wilkins et al., 1999). R_H^{prot} does not depend on

$$R_H^{prot} = \frac{d_{diox}}{d_{prot}} \cdot R_H^{diox} \quad (3)$$

protein concentration at 0% EG, which was shown by repeating the diffusion experiment at 1.5 mM, 0.75 mM, 0.38 mM, and 0.19 mM CspB (data not shown). Therefore, it is unlikely that an aggregation equilibrium distorts the analysis of relaxation parameter (Pfuhl et al., 1999).

R_1, R_2, and *hNOE* spectra (Dayie and Wagner, 1994) and HSQC spectra for the 0% EG sample were recorded at a Bruker DRX500 with spectral widths of 6510 Hz (^{1}H) and 1470 Hz (^{15}N). Spectra at 27% and 70% EG were measured with a Bruker DRX 600 using spectral widths of 9615 Hz and 1764 Hz for ^{1}H and ^{15}N, respectively. Relaxation delays were chosen to ensure that signal intensities of all data sets decayed to zero allowing a two-parameter fit. Therefore, inversion recovery delays at the DRX500 were set to 12.5, 37.7 (two times), 82.9, 148.2, 233.5, 344, 474.6 (two times), 806.1 ms, CPMG delays to 22.8 (two times), 45.6, 68.4, 91.2, 114, 136.8, 159.6, 182.4 (two times), 205.2 ms. At the DRX600, R_1 relaxation delays were set to 10, 40.1 (two times), 130.4, 280.9, 496.6, 767.5, 1103.6 (two times), 1500, 2498.2 ms and R_2 relaxation delays to 22.4 (two times), 44.8, 67.2, 89.6, 112, 134.4, 156.8 (two times), 179.2 ms. For the determination of the heteronuclear NOE effects, two spectra were recorded, one with three seconds of proton saturation and one without. The transverse ^{1}H-^{15}N dipolar/^{15}N CSA cross-correlation rate constants η_{xy} have been derived from the ratio of I_{cross} and I_{auto} measured by a cross-relaxation and an auto-relaxation experiment, respectively (Kroenke et al., 1998). The relaxation delays were set to 32, 53.4, 74.8, 96.1, and 106.8 ms. For I_{cross} between 64 and 96 transients were averaged per t_1 increment, and for I_{auto} between 32 and 64 transients. All data matrices contained 2048 × 512 points.

^{15}*N relaxation parameters (*R_1*,* R_2*, hNOE, and* η_{xy}*)*

R_1 and R_2 rates were derived by fitting a single exponential function (two parameters without offset) to the cross peak intensities using the program GRAFIT (Erithacus software). The used standard error calculated by GRAFIT corresponds to the error derived by a Monte Carlo simulation using CURVEFIT from the MODELFREE program package (Mandel et al., 1995; Palmer et al., 1991) and is about 10% smaller than errors estimated by the jack-knife method. The heteronuclear NOE effect was calculated from the ratios of cross-peak intensities in spectra collected with and without amide proton saturation. The experimental errors around 5% for the heteronuclear NOE effects were estimated from baseline noise in the respective spectra (Nicholson et al., 1992).

The η_{xy} rate constants were determined from a non-least squares fit of Equation 4 to the intensity ratios I_{cross}/I_{auto} at different relaxation times τ using GRAFIT.

$$I_{cross}/I_{auto} = \tanh(\eta_{xy}\tau). \quad (4)$$

The used standard errors from GRAFIT correspond to the errors estimated by Monte Carlo simulations with CURVEFIT and are about 20% above the error using the jack-knife procedure.

Model-free analysis

Calculations of Lipari-Szabo motional parameters were performed with the program MODELFREE (version 3.1). Each set of relaxation parameters at the respective EG concentration was analyzed separately. Relaxation for amide ^{15}N nuclear spins in a diamagnetic protein can generally be described by the dipolar coupling with the directly attached proton and the chemical shift anisotropy of ^{15}N (Abragam, 1961).

$$\begin{aligned} R_1 &= (d_{NH}^2/4)\cdot\{J(\omega_H-\omega_N)+ \\ &\quad 3J(\omega_N)+6J(\omega_H+\omega_N)\}+ \\ &\quad (\omega_N^2/3)(\sigma_{||}-\sigma_\perp)^2 J(\omega_N), \end{aligned} \quad (5)$$

$$\begin{aligned} R_2 &= (d_{NH}^2/8)\cdot\{4J(0)+J(\omega_H-\omega_N)+ \\ &\quad 3J(\omega_N)+6J(\omega_H)+6J(\omega_H+\omega_N)\}+ \\ &\quad (\omega_N^2/18)(\sigma_{||}-\sigma_\perp)^2\{4J(0)+ \\ &\quad 3J(\omega_N)\}+R_{ex}, \end{aligned} \quad (6)$$

$$\begin{aligned} hNOE &= 1+(d_{NH}^2/4R_1)(\gamma_H/\gamma_N)\{6J(\omega_H+ \\ &\quad \omega_N)-J(\omega_H-\omega_N)\} \end{aligned} \quad (7)$$

with

$$d_{NH} = (\mu_0 h\gamma_H\gamma_N/8\pi^2)\langle r_{NH}^{-3}\rangle, \quad (8)$$

where μ_0 is the permeability of free space, h is Planck's constant, γ_H and γ_N are the gyromagnetic ratios of ^{1}H and ^{15}N, respectively, and ω_H and ω_N are the Larmor frequencies of ^{1}H and ^{15}N, respectively. The N-H bond length r_{NH} is 0.102 nm and $\sigma_{||}$ and $\sigma_\perp$ are the parallel and perpendicular components of the ^{15}N chemical shift tensor, which is assumed to be axially symmetric. A conventional value of $\Delta\sigma = \sigma_{||} - \sigma_\perp = -160$ ppm has been used for the Lipari-Szabo analysis (Hiyama et al., 1988). More recently determined values of the ^{15}N chemical shift anisotropy of about −170 ppm (Boyd and Redfield, 1999; Canet et al., 2001; Ottiger et al., 1997) gave no significant variations for τ_m and the derived parameters of internal motion. Slow conformational exchange (R_{ex}) contributes to the transversal relaxation rate R_2.

Table 1. Spectral density functions of the models used for the ^{15}N relaxation data analysis

Model	Spectral density function	Optimized parameters
1	$J(\omega) = 2/5\{S^2\tau_m/(1+\omega^2\tau_m^2)\}$	S^2
2[a]	$J(\omega) = 2/5\{S^2\tau_m/(1+\omega^2\tau_m^2) + (1\text{-}S^2)\tau_e'/(1+\omega^2\tau_e'^2)\}$	S^2, τ_e
3	$J(\omega) = 2/5\{S^2\tau_m/(1+\omega^2\tau_m^2)\}$ $1/T_{2(obs)} = 1/T_2 + R_{ex}$	S^2, R_{ex}
4	$J(\omega) = 2/5\{S^2\tau_m/(1+\omega^2\tau_m^2) + (1\text{-}S^2)\tau_e'/(1+\omega^2\ \tau_e'^2)\}$ $1/T_{2(obs)} = 1/T_2 + R_{ex}$	S^2, τ_e, R_{ex}
5[b]	$J(\omega) = 2/5\{S^2\tau_m/(1+\omega^2\tau_m^2) + S_f^2(1\text{-}S_s^2)\tau_s'/(1+\omega^2\ \tau_s'^2)\}$	S_f^2 ,S_s^2, τ_e

[a] $\tau_e' = \tau_m\ \tau_e/(\tau_m + \tau_e)$.
[b] $\tau_s' = \tau_m\ \tau_s/(\tau_m + \tau_s)$; $S^2 = S_f^2\ S_s^2$.

Spectral density functions $J(\omega_i)$ at the angular frequency ω_i depend on the internal motions of the ^{1}H-^{15}N bond vector and the overall tumbling of the protein. The extended Lipari–Szabo formalism proposes different spectral density functions (Table 1), which depend upon S^2 (the generalized motional order parameter), τ_m (the overall correlation time of rotational diffusion), τ_e (the effective correlation time) and R_{ex} (the rate of chemical or conformational exchange). We used an isotropic model, because the ratio of the three principal inertia axis is 1.0 : 0.92 : 0.77 (derived with pdbinertia from the MODELFREE program package). The model-free analysis was performed by fitting the five models (Table 1) to the determined relaxation parameters at each EG concentration by minimizing the target function of sum-squared error (SSE) for each residue:

$$\begin{aligned} SSE \;=\; & (R_1 - R_1^*)^2/\sigma_1^2 + \\ & (R_2 - R_2^*)^2/\sigma_2^2 + \\ & (hNOE - hNOE^*)^2/\sigma_{hNOE}^2. \end{aligned} \tag{9}$$

R_1, R_2, and *hNOE* represent the experimental relaxation parameters and σ_1, σ_2, and σ_{hNOE} the uncertainties of the experimental data. R_1^*, R_2^*, and *hNOE** are the back-calculated relaxation parameters from the model-free approach using the respective spectral density function given in Table 1. Model selection was achieved by the smallest SSE value to obtain the optimal motional parameter values for each residue. Besides the SSE value, appropriate results for motional parameters such as $\tau_e > 30$ ps, $R_{ex} > 0.5$ s^{-1} and $S_f^2 > 0.9$ are used for model selection. For models with the same SSE value or violation of the other criteria, the simpler model was preferred. The iterative optimization of the overall rotational correlation time τ_m was performed as described by Montelione and coworkers (Feng et al., 1998; Li and Montelione, 1995)

Chemical exchange contributions to R_2

Unimolecular chemical reactions give rise to chemical exchange contributions R_{ex} to the spin-spin relaxation rate R_2 determined by CPMG spin-echo sequences (Carver and Richards, 1972).

$$R_2 = R_2^0 + R_{ex}. \tag{10}$$

A simple approximation of the relaxation rate constant of the resonance associated with site A has been derived independently of assumptions about slow, intermediate, or fast exchange on the NMR chemical shift time scale provided that $p_A \gg p_B$ (Ishima and Torchia, 1999):

$$A \underset{k_{-1}}{\overset{k_1}{\rightleftharpoons}} B, \tag{11}$$

$$\begin{aligned} R_2(1/\tau_{cp}) \;=\; & R_2(1/\tau_{cp} \to \infty) + \\ & p_A p_B \Delta\omega^2 k_{ex}/[k_{ex}^2 + \\ & (p_A^2\Delta\omega^4 + 144/\tau_{cp}^4)^{1/2}]. \end{aligned} \tag{12}$$

In Equations 11 and 12, k_1 and k_{-1} are forward and reverse rate constants and the chemical exchange rate constant $k_{ex} = k_1 + k_{-1}$. p_A and p_B denote the equilibrium populations of equivalent nuclear spins in species *A* and *B* and $\Delta\omega$ represents the difference in the angular frequency between the resonance at site *A* and site

B. τ_{cp} refers to a single spin-echo period ($\tau_{cp}/2 - 180° - \tau_{cp}/2$) during the CPMG sequence.

R_2^0 can be determined experimentally, because interference rate constant η_{xy} of the transverse dipolar and chemical shift anisotropy relaxation is independent of chemical exchange effects (Kroenke et al., 1998; Tjandra et al., 1996).

$$R_2^0 = \sqrt{3}(4c^2 + 3d^2)/(12cd\,P_2[\cos\beta])\eta_{xy} \qquad (13)$$

$$c = \gamma_N B_0 \Delta\sigma/\sqrt{3}, \quad d = -\mu_0\gamma_H\gamma_N/(8\pi^2 r_{NH}^3).$$

B_0 is the static magnetic field strength, −172 ppm was used here for the ^{15}N CSA $\Delta\sigma$, $P_2[x]$=$(3x^2 - 1)/2$, and the experimentally determined angle between the N-H bond vector and the symmetry axis of the ^{15}N chemical shift tensor $\beta = 18.5°$ was used (Boyd and Redfield, 1999; Kroenke et al., 1998; Vugmeyster et al., 2000).

Results

Ethylene glycol does not change the chemical shifts of CspB significantly

To elucidate the influence of EG on the structure of CspB, three ^{1}H-^{15}N HSQC spectra at 0%, 27%, and 70% ethylene glycol were recorded (Figure 1). Although a significant line broadening was detected at increased EG concentrations due to the slower tumbling of the protein molecules at higher viscosity, all cross peaks could directly be assigned in these 2D spectra unambiguously based on the published assignments of CspB (Schnuchel, 1995). For most peaks, a gradual change in chemical shift from 0% to 70% EG was observed (inset in Figure 1). The majority of cross peaks showed chemical shift perturbations in the ^{15}N and ^{1}H dimension smaller than 0.6 ppm and 0.09 ppm, respectively. Therefore we can expect only minor alterations in the three dimensional structure of CspB even at 70% EG, a macroscopic environment which has only 30% of natural water left. This finding was confirmed by uniform far-UV circular dichroism spectra at these EG concentrations (M.H. Jacob, M. Zeeb and J. Balbach, unpublished results). There is no clear correlation between the changes in chemical shifts with secondary structure elements, solvent exposure, and amino acid type or between the perturbation of the respective ^{1}H and ^{15}N chemical shift of the amides.

^{15}N R_1, R_2, and {^{1}H-^{15}N} hNOE relaxation data at various solvent viscosities

Relaxation data for 62, 61, and 56 backbone amides out of 66 non-prolyl residues were obtained at 0%, 27%, and 70% EG, respectively. R_1, R_2 and *hNOE* values of the CspB residues at the respective EG concentration are depicted in Figure 2 and listed in Tables S1–S3 in the Supplementary Material to be obtained from the corresponding author. The average R_1, R_2 and *hNOE* values are 2.11 s^{-1}, 8.19 s^{-1} and 0.63 at 0% EG (500 MHz), 1.23 s^{-1}, 12.77 s^{-1} and 0.72 at 27% EG (600 MHz), and 0.76 s^{-1}, 17.96 s^{-1}, and 0.67 at 70% EG (600 MHz), respectively. Transverse relaxation rates at 70% EG exhibit large uncertainties because of a low signal-to-noise ratio in the spectra. Averaged R_1 values decrease and averaged R_2 values increase at increasing solvent viscosity as expected from a reduced tumbling rate of CspB in the EG containing solvents.

Overall rotational correlation time and backbone dynamics of CspB

The overall tumbling of the protein molecules can be described by the rotational correlation time τ_m, which is proportional to the viscosity of the solvent for a spherical rigid body (Einstein, 1905). A detailed analysis of τ_m and the backbone dynamics of CspB at various solvent viscosities were achieved by an extended Lipari–Szabo analysis (Clore et al., 1990; Lipari and Szabo, 1982a, b) of the R_1, R_2 and *hNOE* relaxation parameters. Using an isotropic tumbling model (see Experimental procedures) we performed an iterative optimization schedule as described by Montelione and coworkers (Feng et al., 1998; Li and Montelione, 1995). Model selection and the results of the optimized motional parameters determined by the Lipari-Szabo analysis depend significantly on the initial value of the overall correlation time τ_m. The latter can be overestimated for example if the R_2 values include large chemical exchange contributions. Table 2 summarizes the different optimization cycles starting with an initial estimate of τ_m based on the average $\langle R_2/R_1 \rangle$ of all analyzed residues. The criteria for exclusion of residues to improve the estimate of the overall correlation time for every MODELFREE cycle are given in the legend of Table 2.

The iteratively refined τ_m times of CspB at three different EG concentrations show a remarkably linear increase from 4.4 ns to 17.3 ns between 0% and 70% EG (Figure 3A). Plotting the relative rotational

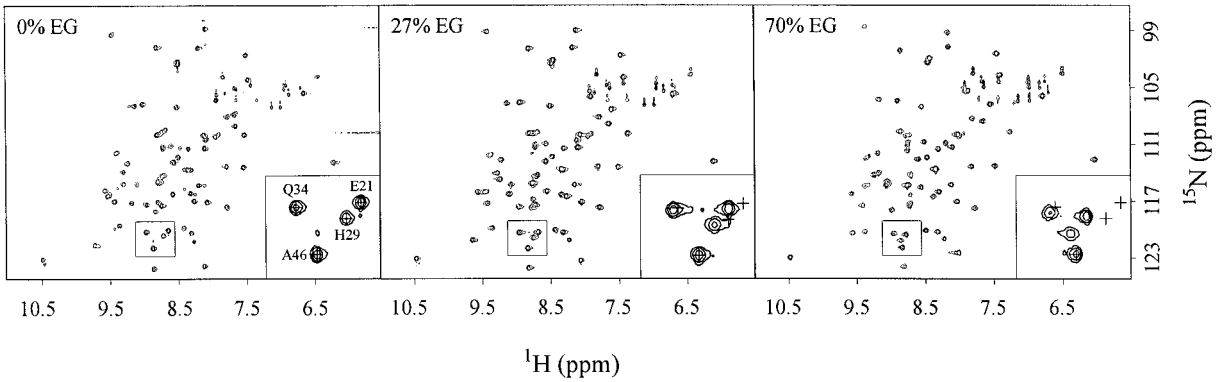

Figure 1. Contour plots of 2D ^{1}H-^{15}N HSQC spectra of CspB at 0%, 27%, and 70% ethylene glycol at 25 °C. NMR samples contained 1.5 mM protein dissolved in 100 mM Na-cacodylate/HCl buffer with 7% D_2O at pH 7.0 and the respective amount of ethylene glycol. The insets enlarge the indicated section including four cross peaks. Their chemical shift positions at 0% EG are indicated by a cross in all three insets.

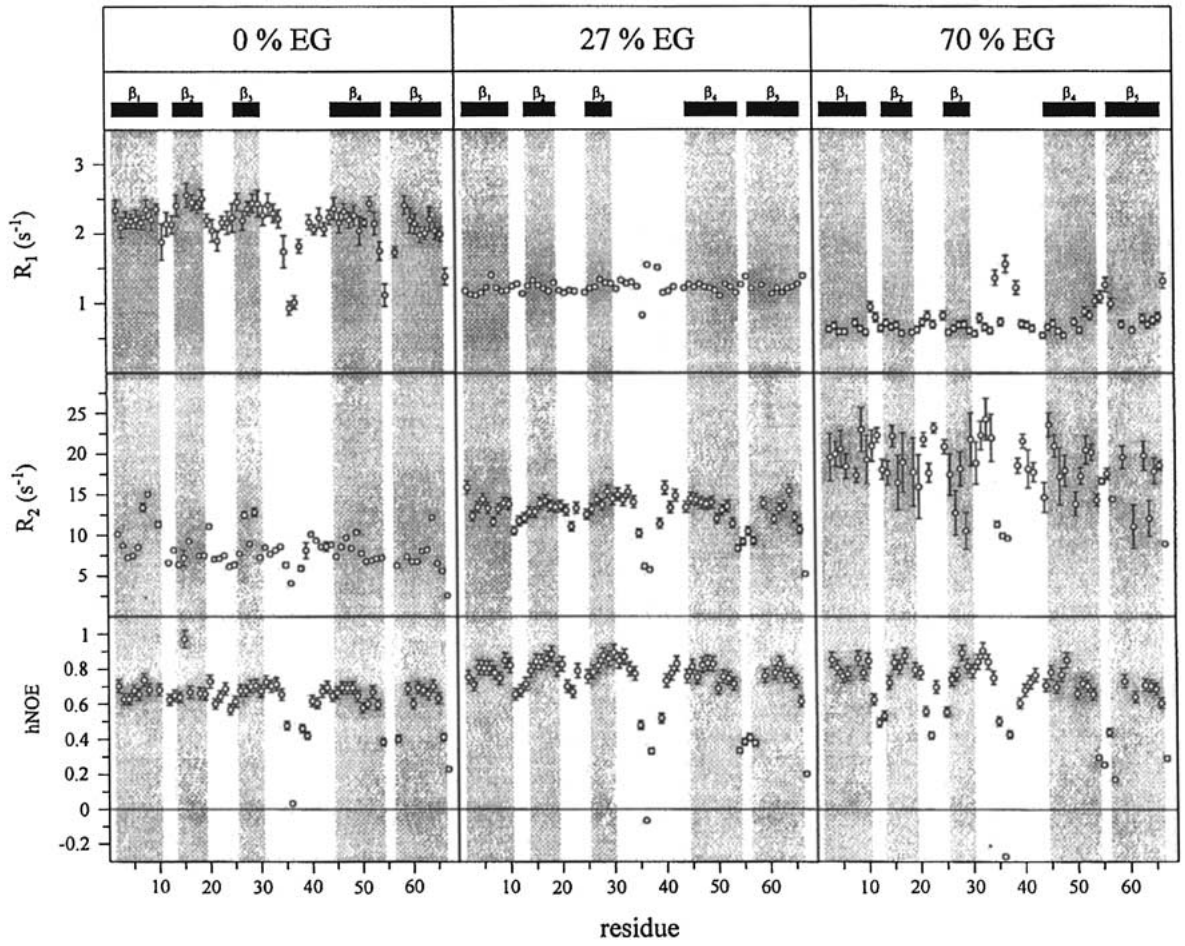

Figure 2. ^{15}N R_1- and R_2-rates as well as heteronuclear NOE effects at 0% EG, 27% EG, and 70% EG. The relaxation data were recorded at 50.7 MHz (0% EG) and 60.8 MHz (27% and 70% EG) nitrogen resonance frequency. Black and grey bars indicate residues, which form the five β-strands.

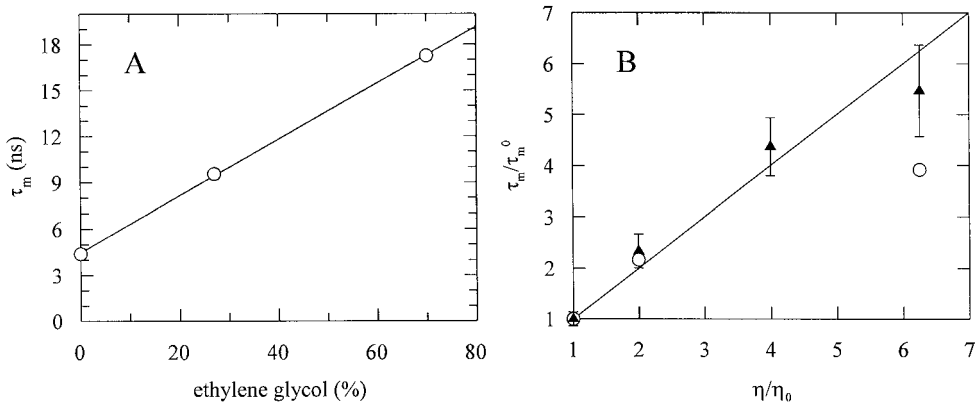

Figure 3. (A) Overall correlation times τ_m at different EG concentrations derived from the ^{15}N relaxation data of CspB using the model-free approach. The line represents a linear fit of the three data points. (B) Relative overall correlation times derived from (○) the ^{15}N relaxation data and (▲) the diffusion experiments at different relative viscosities. The line with slope 1 indicates the theoretical viscosity dependence of the correlation time from the Stokes–Einstein equation. Missing bars indicate that the symbol size exceeds the error.

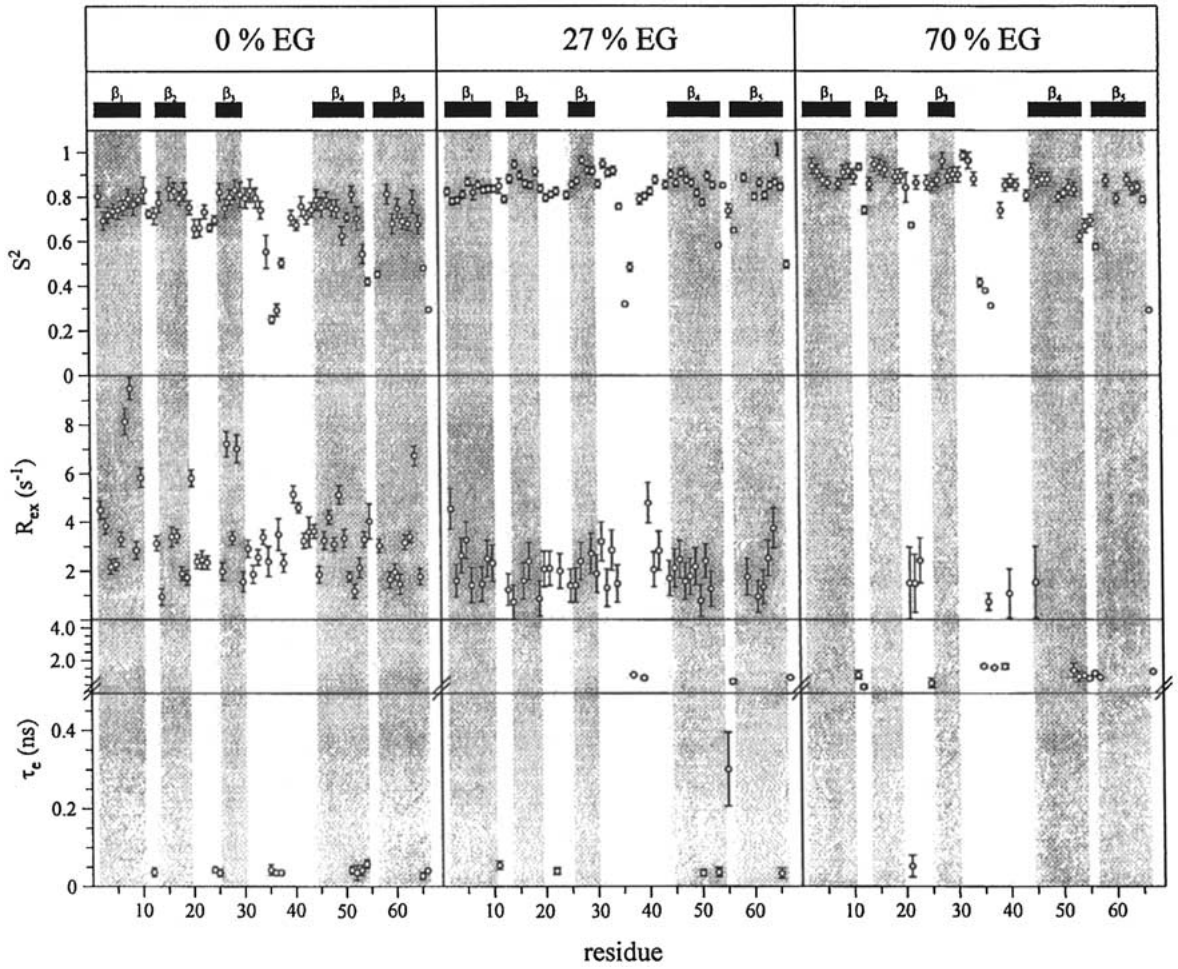

Figure 4. Generalized order parameters S^2, chemical exchange contributions R_{ex} and effective correlation times τ_e of CspB at 0% EG, 27% EG, and 70% EG revealed from the extended model-free analysis of the relaxation data of Figure 2. Error bars are given according to the Monte Carlo simulations in MODELFREE. Black and grey bars indicate residues, which form the five β-strands.

Table 2. Iterative optimization of averaged R_2/R_1 ratios and corresponding overall rotational correlation times τ_m of CspB at 25 °C under various solvent viscosities

Sample	Cycle	$\langle R_2/R_1\rangle$[a]	$\tau_{m,init}$ (ns)	$\tau_{m,opt}$ (ns)
CspB in		3.90[b] ± 0.87	6.44 ± 1.12	
0% EG	0	3.74[c] ± 0.25	6.27 ± 0.30	6.27 ± 0.05
	1	3.60[d] ± 0.17	6.12 ± 0.24	6.02 ± 0.05
	2	3.26[e] ± 0.18	5.67 ± 0.28	5.48 ± 0.06
	3	3.00[f] ± 0.03	5.32 ± 0.03	5.21 ± 0.02
	4	2.86[g] ± 0.01	5.12 ± 0.02	4.34 ± 0.03
	5	2.38[h] ± 0.01	4.35 ± 0.02	4.32 ± 0.02
CspB in		10.45[b] ± 3.85	9.90 ± 0.53	
27% EG	0	11.00[c] ± 0.69	10.20 ± 0.27	10.11 ± 0.04
	1	10.85[d] ± 0.66	10.12 ± 0.24	9.90 ± 0.03
	2	10.51[e] ± 0.56	9.95 ± 0.28	9.76 ± 0.05
	3	9.90[f] ± 0.59	9.59 ± 0.28	9.56 ± 0.06
CspB in		25.31[b] ± 7.72	15.92 ± 2.46	
70% EG	0	27.91[c] ± 2.84	16.83 ± 0.89	17.39 ± 0.15
	1	29.60[d] ± 1.95	17.28 ± 0.58	17.27 ± 0.12

[a]The value $\langle R_2/R_1\rangle$ is the mean ratio of R_2/R_1.
[b]The initial value of $\langle R_2/R_1\rangle_{all}$ averaged over all 62 (0% EG), 61 (27% EG) or 56 (70% EG) analyzed amides.
[c]$\langle R_2/R_1\rangle$ for 48, 45 or 47 amides for 0%, 27% or 70% EG, respectively, that satisfy the criteria $|R_2/R_1\text{-}\langle R_2/R_1\rangle_{all}| < 1$ (0% EG), <1.5 (27% EG), <3 (70% EG). The excluded residues are K7, W8, G14, V20, D24, D25, F27, H29, G37, V52, N55, T64, E66, A67 (0% EG), L2, K5, K7, S31, G35, E36, G37, K39, T40, G54, N55, R56, G57, T64, E66, A67 (27% EG) or F27, H29, G35, E36, G37, K39, A61, T64, A67 (70% EG).
[d]$\langle R_2/R_1\rangle$ for 39 (0% EG), 41 (27% EG) or 40 (70% EG) amides from cycle 0 that were fit with R_{ex} <1.5 Hz. Therefore, additional to footnote c excluded amides are L2, E3, N10, G35, E36, T40, L41, F49, G57 (0% EG), G4, S11, I33, E42 (27% EG) or F9, E21, Q23, I33, T40, Q45, R56 (70% EG).
[e]All of the R_2 values were corrected by subtracting the R_{ex} values calculated in cycle 1: $R_{2,corr} = R_2\text{-}R_{ex}$. The resulting $\langle R_2/R_1\rangle_{all,corr}$ values are 3.26 ± 0.18 (0% EG) or 9.97 ± 2.78 (27% EG). $\langle R_2/R_1\rangle$ was derived using 44 (0% EG) or 53 (27% EG) amides which obey the criteria $|(R_2/R_1)_{corr}\text{-}\langle R_2/R_1\rangle_{all,corr}| < 0.36$ (0% EG) or <2.78 (27% EG). The excluded residues are F9, N11, G14, D24, D25, G35, E36, G37, F38, T40, G44, E50, V52, G54, G57, A66, A67 at 0% EG and E36, G37, K39, G54, N55, R56, G57, A67 at 27% EG.
[f]The same criteria was used as in footnote e using the R_{ex} values of cycle 2 for R_2 correction ($\langle R_2/R_1\rangle)_{all,corr}$ of 2.51 ± 0.20 or 9.56 ± 2.18 (or 0% or 27% EG, respectively). $\langle R_2/R_1\rangle$ values were calculated with 53 or 56 amides for 0% or 27% EG, respectively. The excluded residues are N11, D24, G35, E36, G37, F38, G54, G57, A67 for 0% EG or E36, G37, G54, N55, A67 for 27% EG.
[g]The same criteria was used as in footnote e using the R_{ex} values of cycle 3 for R_2 correction ($\langle R_2/R_1\rangle_{all,corr} = 2.82 \pm 0.20$). $\langle R_2/R_1\rangle$ values were calculated with 43 amides for 0% EG excluding residues N11, G16, I18, D24, V26, G35, E36, G37, F38, Q45, E50, E53, G54, N55, G57, Q59, A60, A61, A67.
[h]The same criteria was used as in footnote e using the R_{ex} values of cycle 4 for R_2 correction ($\langle R_2/R_1\rangle_{all,corr} = 2.36 \pm 0.10$). $\langle R_2/R_1\rangle$ values were calculated with 49 amides for 0% EG excluding residues N11, G14, D24, G35, E36, G37, F38, V52, G54, N55, G57, E66, A67.

correlation time τ_m/τ_m^0 as a function of the solvent viscosity relative to water (η/η_0), however, reveals a deviation from linearity at 70% EG (open circles in Figure 3B). The retarded tumbling of the 67 amino acid residue CspB at 27% and 70% EG mimics about the rotational correlation time of a 170 and 340 amino acid protein in water, respectively. This is basically the reverse approach of encapsulating proteins in reverse

micelles and dissolving them in low-viscosity fluids (Wand et al., 1998).

The motional parameters derived from the extended Lipari–Szabo analysis (S^2 and R_{ex}) of CspB at the studied solvent viscosities are depicted in Figure 4. There are significant differences in the number of best fit models for the three EG concentrations listed in Table 3. At 0% EG most selected models include chemical exchange terms R_{ex} (model 3). At higher solvent viscosities, simpler models are sufficient to interpret the relaxation data and at 70% EG model 1 dominates. Only a marginal number of backbone amides required model 5, which assumes a multiple time scale model of the internal motions (Table 3).

The generalized order parameters are predominantly independent of viscosity indicating that the amplitudes of internal motions are mainly independent from the overall tumbling of CspB (Figure 4). Most residues comprised in the five β-strands show S^2 values above 0.75 indicating a reduced flexibility of these regions on a sub-nanosecond time scale. Slightly reduced order parameters were obtained for some backbone amides in the loops between β-strands β_1/β_2 and β_2/β_3. Significantly reduced S^2 values as small as 0.25, indicating large scale internal motion amplitudes, were determined for the long loops between β-strands 3 and 4 and between β-strands 4 and 5 as well as for the C-terminus.

The chemical or conformational exchange contribution R_{ex} to the R_2 relaxation rate is substantial at low solvent viscosities (0% and 27% EG) throughout the whole protein chain (Figure 4). R_{ex} contributions remain to be seen in the flexible loops between strands β2/β3 and β3/β4 up to 70% EG. The total number of residues revealing R_{ex} terms decreases from 55 at 0% EG to 6 at 70% EG (see Table 3).

Effective correlation times τ_e account for additional fast internal motions of the protein. At the lowest solvent viscosity, backbone amides τ_e contributions range around 50 ps. With increasing solvent viscosity τ_e values of most of these residues shift values above 500 ps.

It should be mentioned that the dynamic parameters S^2, τ_e, and R_{ex} of the structurally homologous CspA protein from *Escherichia coli* show very similar variations along the peptide backbone compared to CspB at 0% EG (Feng et al., 1998; Li and Montelione, 1995). CspA has a three residues extension at the N terminus, where the lowest order parameters were found.

Table 3. Number for best-fit models for CspB at various solvent viscosities after the iterative optimization of the overall correlation time τ_m

Model	0% EG	27% EG	70% EG
1	2	8	38
2	5	8	7
3	48	41	5
4	7	1	1
5	0	3	5

Translational diffusion and hydrodynamic radii of CspB at various solvent viscosities

The Stokes–Einstein equation ($D = kT/(6\pi r\eta)$) describes the viscosity (η) dependence of the diffusion constant (D) of a spherical body (with radius r) in a continuous fluid at a given temperature (T). The use of the effective hydrodynamic radius R_H extends the equation to more complex systems, where R_H is the radius of a sphere with the same diffusion coefficient. We determined R_H of CspB by NMR diffusion measurements employing the PG-SLED pulse sequence. Dioxan was used as an internal reference to estimate R_H (Balbach, 2000; Wilkins et al., 1999) because it does neither interact significantly with folded nor denatured polypeptide chains (Jones, 1997). Table 4 summarizes the radii of CspB at four different solvent viscosities. The internal referencing with dioxan corrects as expected for the decreased diffusion at higher solvent viscosities leading to a uniform R_H of CspB at all four EG concentrations within experimental error. For a comparison with the rotational correlation times derived from the ^{15}N relaxation analysis, the hydrodynamic radii were converted into correlation times (τ_m^{diff}) by the Stokes–Einstein–Debye equation ($\tau_m^{diff} = 4\pi R_H^3\eta/(3kT)$) (Debye, 1929) and plotted in Figure 3B with filled triangles. The relative correlation times τ_m/τ_m^0 from the diffusion experiments follow approximately the expected linear increase with relative solvent viscosity.

Experimental determination of R_{ex} contributions to R_2

For the experimental verification of the chemical exchange contributions R_{ex} to the transversal relaxation rates, we determined R_2^0 from the transverse ^1H-^{15}N dipolar /^{15}N chemical shift anisotropy relaxation interference. The difference between R_2 and R_2^0 (giving R_{ex}

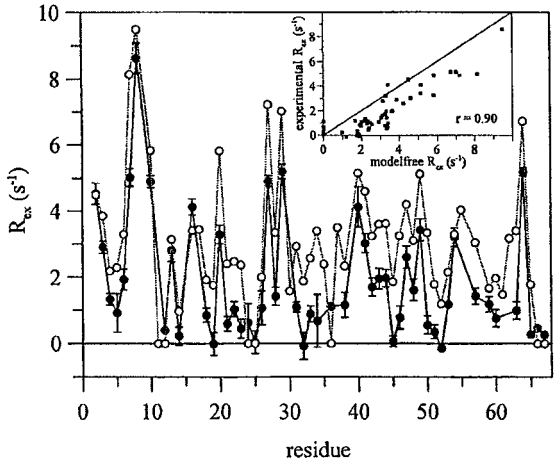

Figure 5. Comparison of the chemical exchange rates of CspB residues derived by (○) the Lipari–Szabo approach or (●) by the dipolar/CSA relaxation interference. Error bars are only given for the latter R_{ex} values for clarity. They have been derived by error propagation of the errors of R_2 and R_2^0. Grey lines connect the open symbols and black lines connect filled symbols. The small inset shows a correlation of the R_{ex} values derived from both methods and a line with a slope of 1.

according to Equation 10) is plotted for the residues of CspB at 0% EG with black filled symbols in Figure 5. There is a significant correlation (r = 0.90) between the experimentally derived chemical exchange rates and the rates determined by the model-free approach (open symbols in Figure 5).

Discussion

For a detailed investigation of the dynamics of the cold shock protein CspB, we determined ^{15}N relaxation rates at various solvent viscosities. This approach increases in principle the experimentally accessible amount of data at constant magnetic field strength and temperature to derive elaborate parameters of motion from proteins. The solvent viscosity was adjusted by ethylene glycol, which does not affect the structure of CspB up to 70% EG, corresponding to an increase of the macroscopic viscosity by a factor of 6.

Solvent viscosity versus microviscosity

The overall rotational correlation time τ_m is a sensitive measure of the microviscosity, which determines the tumbling of the protein molecules. The Stokes-Einstein equation predicts that the relative correlation time increases with the relative solvent viscosity with a slope of one. This was indeed observed for CspB between 0% and 27% EG ($\eta/\eta_0 = 2$). At 70% EG ($\eta/\eta_0 = 6$), however, the correlation time is much smaller than predicted, i.e. the protein tumbles faster than expected from the macroscopic viscosity. We can exclude that this apparent faster tumbling results from a shift of the equilibrium between unfolded and folded CspB molecules towards the folded population by the stabilizing effect of EG, because only 1% of the molecules are unfolded at 0% EG. We suggest instead that the microviscosity within the hydration shell of CspB is smaller than the bulk solvent viscosity. As a control, we calculated the relative correlation times from the hydrodynamic radius of CspB derived from translational diffusion experiments (Figure 3B). Dioxan was used as internal standard, where we have to assume that its reference radius R_H^{diox} is not affected by EG (Jones et al., 1997). We found a uniform R_H for CspB at four different EG concentrations (Table 4) within the experimental error, which confirms our assumptions. The absolute value of the calculated correlation times from these hydrodynamic radii by the Stokes–Einstein–Debye equation (τ_m^{diff}) in pure water is about 30% below the value derived from the ^{15}N relaxation rates, which might result from an overestimation of R_H^{diox} by Wilkins et al. (1999). Due to the small R_H variations of CspB with viscosities, the relative correlation times calculated from the diffusion experiments ($\tau_m^{diff}/\tau_m^{diff0}$) are proportional to the bulk viscosity within experimental error. This indicates that the microviscosity within the hydration shell rather than the size of the protein plus hydration shell determines the rotational tumbling.

Similar deviations of the rotational correlation times from the Stokes–Einstein equations have been observed by time-resolved absorption or fluorescence anisotropy experiments of proteins in viscous media (Lakshmikanth and Krishnamoorthy, 1999; Lavalette et al., 1999). Seewald et al. (2000) studied the B1 domain of *Streptococcal* protein G between 0 °C and 50 °C at six different temperatures by ^{15}N NMR relaxation and extended Lipari–Szabo analyses. The relative viscosity increases between 50 °C and 0 °C by a factor of three. If we assume a linear increase of τ_m with the temperature between 50 °C and 0 °C, the rotational correlation time at 0 °C ($\eta/\eta_0 = 3$) is still 25% below the expected value (Seewald et al., 2000). The authors could exclude in this study significant contributions from chemical exchange by comparing the R_2 rates and the transverse cross-relaxation rates η_{xy} and could therefore exclude a possible bias of τ_m

Table 4. Hydrodynamic radii of CspB at different solvent viscosities

%EG	η (mPa·s)[a]	d_{prot}	d_{ref}	R_H (Å)	τ_m^{diff} (ns)[b]
0	1.01	3.07 ± 0.10	20.65 ± 0.06	14.3 ± 0.5	3.0 ± 0.3
27	1.99	1.76 ± 0.06	12.55 ± 0.08	15.1 ± 0.5	7.0 ± 0.7
52	4.12	1.58 ± 0.04	10.86 ± 0.04	14.6 ± 0.4	13.1 ± 1.1
70	6.25	1.26 ± 0.03	8.17 ± 0.07	13.7 ± 0.6	16.4 ± 2.2

[a]Solvent viscosities were measured with an oscillating capillary rheometer (Jacob et al., 1997).
[b]τ_m^{diff} was calculated with the Stokes-Einstein-Debye equation $\tau_m^{diff} = 4\pi R_H^3 \eta/(3kT)$.

Table 5. Calculated chemical exchange contributions R_{ex}^a to R_2 from the protein folding rates of CspB at various EG concentrations

Residue	$\Delta\delta_N$ (ppm)	R_{ex} at 0% EG (s^{-1})	R_{ex} at 27% EG (s^{-1})	R_{ex} at 70% EG (s^{-1})
W8	11.7	9.9 (9.5)[b]	1.7 (1.5)	0.1 (−)[c]
V20	6.8	4.7 (5.8)	0.8 (0.9)	0.0 (−)
F27	8.0	6.1 (7.2)	1.0 (1.2)	0.1 (−)

[a]Equation 12 was used to calculate the R_{ex} contributions to R_2 with the experimentally used $\tau_{cp} = 1$ ms and the following folding rates (Jacob et al., 1997; Schindler et al., 1995): $k_f = 1070\ s^{-1}$ and $k_u = 14\ s^{-1}$ at 0% EG, $k_f = 1000\ s^{-1}$ and $k_u = 2.3\ s^{-1}$ at 27% EG, and $k_f = 160\ s^{-1}$ and $k_u = 0.1\ s^{-1}$ at 70% EG.
[b] The number in brackets represents the R_{ex} value derived from the extended Lipari–Szabo analysis (Figure 4).
[c]The extended Lipari–Szabo analysis revealed model 1 for all three residues at 70% EG and therefore no R_{ex} contributions to R_2.

according to changes of the R_{ex} contributions to R_2 at increased solvent viscosities.

Protein hydration and preferential hydration of CspB in water/EG mixtures

Ethylene glycol and polyols in general stabilize proteins due to preferential hydration of the native state compared to the unfolded state (Gekko, 1982; Timasheff, 1992, 2002). Therefore, the stability of CspB increases between 0% and 30% EG by about 5 kJ/mol (Jacob et al., 1997). At higher EG concentrations, no further stabilization was observed. In other words at higher EG concentrations no further preferential hydration of the folded state occurs compared to the unfolded state. The EG dependence of the rotational correlation time τ_m presented here reflects another concept, the difference in the solvent-cosolvent composition in the bulk solution and at the protein surface of the native state, i.e., protein hydration (Timasheff, 2002). Nevertheless, some qualitative conclusions are possible. At 27% EG, the cosolvent content at the surface of CspB still represents the bulk solvent because of the linear increase of τ_m expected from the Stokes–Einstein equation. At 70% EG, the faster tumbling of CspB than expected from the bulk solvent indicates a higher water content in the hydration shell than 30%.

Concomitant with the stabilization of CspB at increasing EG concentrations, both un- and refolding get retarded (Jacob et al., 1997). This retardation scales linearly with the solvent viscosity up to 27% EG but becomes progressively stronger at higher viscosities resulting in 25-fold decelerated folding at a relative viscosity of 6. A constant hydrodynamic radius of CspB at different EG concentrations proves that CspB remains monomeric under this conditions excluding oligomerization as possible reason for strongly decelerated folding. One possible explanation for this retardation came from pressure-jump and high-pressure stopped-flow fluorescence experiments, which revealed a very small but positive activation volume for both, the un- and refolding reaction of CspB (Jacob et al., 2002). The authors conclude that the influx of water during the rate-limiting event of unfolding gets possibly hindered by a high EG concentration at the surface of CspB, which is not supported by our results. An alternative explanation for retarded un- and refolding would be that the transition state of folding shows higher preferential hydration compared to the native and unfolded state. It should be

noted that a protein solved in 30% water and 70% EG is a complex mixture with strongly deviating activity coefficients from unity (Suleiman and Eckert, 1994). For protein stability and kinetic protein folding studies in such mixtures additionally the unfolded state and the transition state of folding have to be considered. Therefore, the strong deviations from linearity of the decreasing rotational tumbling, the decreasing stabilization of CspB, and the retardation of protein folding at very high EG concentrations above 30% originate possibly from different phenomena, which need to be further investigated.

Internal motion of CspB at various solvent viscosities

An extended Lipari–Szabo analysis at three different solvent viscosities allows an insight into the internal motions of CspB. One of the prerequisites of this model-free approach is the independence of overall tumbling and internal motion (Lipari and Szabo, 1982a). The overall tumbling varies between 4.32 ns and 17.3 ns at the respective EG concentrations. Many ^{15}N relaxation studies showed that among the five parameters to describe internal motion (S^2, R_{ex}, τ_e, S_f^2, and S_s^2) the most reliable results come from the order parameter S^2 independent of the problem to find the adequate model for the spectral density function for each residue from statistical valuations (Palmer, 2001). We found a consistent picture of the amplitudes of subnanosecond internal motions at all solvent viscosities for the respective secondary structure elements of CspB (S^2 values in Figure 4). Large amplitudes were found for the long loops between β-strand 3 and 4 as well as β-strand 4 and 5 and for the C-terminus independent from the solvent viscosity.

In contrast, the derived correlation times for internal motion (τ_e values is Figure 4) varied at different EG concentrations. τ_e is much less well defined by NMR relaxation measurements compared to S^2 with typical errors up to 30–50%, especially when relaxation data were recorded at only a single magnetic field strength. The spectral density functions of model 2 and model 4 (Table 1) reflect that τ_e values below 5% of the overall correlation time τ_m as well as τ_e values close to τ_m are poorly defined (Ernst et al., 1996). Therefore, the absolute value of τ_m determines the range, where τ_e contributes to the spectral density function. This explains why at 0% EG the majority of the τ_e times range around 50 ps. The 'observation window' shifts up at 70% EG, where basically all picosecond contributions vanish and the internal nanosecond motions are well defined. As expected, they are located in the loop regions between the five β-strands and at the C-terminus. We did not observe a gradual shift of the internal correlation times with an increasing EG concentration. Therefore, we assume that EG does not affect the internal motion.

A similar approach of shifting the 'observation window' of τ_e by changing τ_m via the solvent viscosity has been followed by Lienin et al. to analyze the ^{13}C relaxation of 1,3-dibromoadamantane in polychlorotrifluoroethene (Lienin et al., 1998). Unfortunately, the authors found a heterogeneous environment leading to at least two populations of molecules tumbling on a nano- and picosecond time range, respectively, and could therefore not prove the principles of this approach.

Millisecond motions of CspB originate from protein folding

Chemical exchange contributions to the ^{15}N R_2 rates can be determined indirectly by an extended Lipari-Szabo analysis, where R_{ex} is the difference between the experimental R_2 rates and the expected contribution from the fast motions on a nano- to picosecond time scale (Equation 6). We determined the latter contribution (R_2^0) experimentally at 0% EG from the transverse ^{1}H-^{15}N dipolar/^{15}N chemical shift anisotropy relaxation interference and found a good correlation for the derived R_{ex} rates by these two methods.

Recent studies proved that very high protein folding rates on a millisecond time scale give rise to these chemical exchange terms and that R_{ex} rates from relaxation studies can be used for quantitative measurements of ultra fast protein folding rates (Burton et al., 1996; Mulder et al., 2001; Tollinger et al., 2001; Vugmeyster et al., 2000). Therefore, we calculated the expected R_{ex} rates for three residues of CspB from the known protein folding rates at 0%, 27%, and 70% EG (Jacob et al., 1997; Schindler et al., 1995) using the second right term of Equation 12. For these residues, we can estimate the difference in chemical shifts $\Delta\delta_N$ between folded and unfolded state from a ^{15}N ZZ-exchange experiment (Farrow et al., 1994) at 3M urea (data not shown). Although we had to assume urea independent $\Delta\delta_N$ shifts, the calculated and experimentally derived R_{ex} rates at 0M urea correspond well (Table 5).

EG stabilizes CspB at 25 °C and decreases both, the un- and refolding rates (Jacob et al., 1997). Therefore, the population of unfolded molecules drops with

increasing EG concentrations (1.3% at 0% EG, 0.2% at 27% EG and 0.06% at 70% EG). Together with the decreased folding rates, we expected no R_{ex} contribution from protein folding at 70% EG. Table 3 and Figure 4 show indeed decreased R_{ex} rates at 27% EG and only 6 remaining residues with R_{ex} contributions at 70% EG. Although we had much bigger uncertainties for the experimental R_2 rates at 70% EG due to the slower tumbling of the protein molecules (Figure 2), the overall rotational correlation time could be optimized in only one iteration cycle (Table 2), which is another indication for missing R_{ex} contributions to R_2 at very high EG concentrations.

Conclusions

In the present study we could show that a variation of the solvent viscosity increases the amount of ^{15}N relaxation data to reveal a more detailed picture of the dynamics of proteins. The deviation of the rotational correlation time from linearity towards a faster Brownian motion at 70% EG might be explained by strong water hydration of the cold shock protein preventing the uptake of 70% EG into the hydration shell. Therefore, the rotational correlation time serves as a sensitive measure for the local microviscosity. The amplitudes of internal motions on a sub-nanosecond time scale are only marginally affected if the overall tumbling decreases by a factor of 4. This proves the independence of internal and overall motion of the cold shock protein. The bulk viscosity allows to determine the time scale, where the internal correlation time contributes significantly to the spectral density function. In the special case of CspB, protein folding rates on a millisecond time scale give rise to different chemical exchange contributions to R_2 at different ethylene glycol concentrations. For most proteins, protein folding does not contribute to R_{ex} due to the low population of the unfolded state and lower folding rates. Therefore, a joint fit of all relaxation data at different viscosities should be feasible and a variation of the magnetic field strength or the temperature to increase the amount of input data for fitting could be avoided. A higher amount of relaxation data determined for one protein leads to a more reliable model selection and decreasing errors for the parameters of internal motion. Finally, the use of small proteins at high solvent viscosities mimics the tumbling of much larger proteins, which might help to setup NMR experiments for large proteins.

Acknowledgements

This research was supported by grants from the Deutsche Forschungsgemeinschaft (Ba 1821/2-1; Ba 1821/3-1) and INTAS 2001-2347. We thank M.J. Seewald, K. Schweimer, and F.X. Schmid for helpful discussions and P. Rösch for measuring time at the DRX600 NMR spectrometer.

References

Bai, Y.W., Milne, J.S., Mayne, L. and Englander, S.W. (1994) *Proteins Struct. Funct. Genet.*, **20**, 4–14.
Balbach, J. (2000) *J. Am. Chem. Soc.*, **122**, 5887–5888.
Boyd, J. and Redfield, C. (1999) *J. Am. Chem. Soc.*, **121**, 7441–7442.
Burton, R.E., Huang, G.S., Daugherty, M.A., Fullbright, P.W. and Oas, T.G. (1996) *J. Mol. Biol.*, **263**, 311–322.
Canet, D., Barthe, P., Mutzenhardt, P. and Roumestand, C. (2001) *J. Am. Chem. Soc.*, **123**, 4567–4576.
Carver, J.P. and Richards, R.E. (1972) *J. Magn. Reson.*, **6**, 89–105.
Clore, G.M., Szabo, A., Bax, A., Kay, L.E., Driscoll, P.C. and Gronenborn, A.M. (1990) *J. Am. Chem. Soc.*, **112**, 4989–4991.
Dayie, K. and Wagner, G. (1994) *J. Magn. Reson. A*, **111**, 121–126.
Debye, P. (1929). *Polar Molecules*, Dover, New York.
Einstein, A. (1905) *Ann. Phys.*, **17**, 549–560.
Ernst, R.R., Blackledge, M.J., Bremi, T., Brüschweiler, R., Ernst, M., Griesinger, C., Mádi, Z.L., Peng, J.M., Schmid, J.M. and Xu, P. (1996) In *NMR as a Structural Tool for Macromolecules: Current Status and Future Directions*, Rao, B.D.N. and Kempleeds, M.D. (Eds.), Plenum Press, New York, pp. 15–30.
Farrow, N.A., Zhang, O., Forman-Kay, J.D. and Kay, L.E. (1994) *J. Biomol. NMR*, **4**, 727–734.
Feng, W., Tejero, R., Zimmerman, D.E., Inouye, M. and Montelione, G.T. (1998) *Biochemistry*, **37**, 10881–10896.
Gekko, K. (1982) *J. Biochem.*, **91**, 1197–1204.
Gibbs, S.J. and Johnson, Jr., C.S. (1991) *J. Magn. Reson.*, **93**, 395–402.
Ishima, R. and Torchia, D.A. (1999) *J. Biomol. NMR*, **14**, 369–372.
Jacob, M., Geeves, M., Holtermann, G. and Schmid, F.X. (1999) *Nat. Struct. Biol.*, **6**, 923–926.
Jacob, M., Schindler, T., Balbach, J. and Schmid, F.X. (1997) *Proc. Natl. Acad. Sci. USA*, **94**, 5622–5627.
Jacob, M.H., Saudan, C., Holtermann, G., Martin, A., Perl, D., Merbach, A.E. and Schmid, F.X. (2002) *J. Mol. Biol.*, **318**, 837–845.
Jones, J.A., Wilkins, D.K., Smith, L.J. and Dobson, C.M. (1997) *J. Biomol. NMR*, **10**, 199–203.
Kroenke, C.D., Loria, J.P., Lee, L.K., Rance, M. and Palmer, A.G., III (1998) *J. Am. Chem. Soc.*, **120**, 7905–7915.
Lakshmikanth, G.S. and Krishnamoorthy, G. (1999) *Biophys. J.*, **77**, 1100–1106.
Lavalette, D., Tetreau, C., Tourbez, M. and Blouquit, Y. (1999) *Biophys. J.*, **76**, 2744–2751.
Li, Y.C. and Montelione, G.T. (1995) *Biochemistry*, **34**, 2408–2423.
Lienin, S.F., Büschweiler, R. and Ernst, R.R. (1998) *J. Magn. Reson.*, **131**, 184–190.
Lipari, G. and Szabo, A. (1982a) *J. Am. Chem. Soc.*, **104**, 4546–4559.
Lipari, G. and Szabo, A. (1982b) *J. Am. Chem. Soc.*, **104**, 4559–4570.

Mandel, A.M., Akke, M. and Palmer, III, A.G. (1995) *J. Mol. Biol.*, **246**, 144–163.

Mulder, F.A., Mittermaier, A., Hon, B., Dahlquist, F.W. and Kay, L.E. (2001) *Nat. Struct. Biol.*, **8**, 932–935.

Nicholson, L.K., Kay, L.E., Baldisseri, D.M., Arango, J., Young, P.E., Bax, A. and Torchia, D.A. (1992) *Biochemistry*, **31**, 5253–5263.

Ottiger, M., Tjandra, N. and Bax, A. (1997) *J. Am. Chem Soc.*, **119**, 9825–9830.

Palmer, III, A.G. (1997) *Curr. Opin. Struct. Biol.*, **7**, 732–737.

Palmer, III, A.G. (2001) *Annu. Rev. Biophys. Biomol. Struct.*, **30**, 129–155.

Palmer, III, A.G., Kroenke, C.D. and Loria, J.P. (2001) *Meth. Enzymol.*, **339**, 204–238.

Palmer, III, A.G., Rance, M. and Wright, P.E. (1991) *J. Am. Chem. Soc.*, **113**, 4371–4380.

Peng, J.W. and Wagner, G. (1992) *Biochemistry*, **31**, 8571–8586.

Pfuhl, M., Chen, H.A., Kristensen, S.M. and Driscoll, P.C. (1999) *J. Biomol. NMR*, **14**, 307–320.

Sambrook, J., Fritsch, E.F. and Maniatis, T. (1989) *Molecular Cloning: A Laboratory Manual*, Cold Spring Harbor Laboratory Press, Cold Spring Harbor, NY.

Schindler, T., Herrler, M., Marahiel, M.A. and Schmid, F.X. (1995) *Nat. Struct. Biol.*, **2**, 663–673.

Schnuchel, A. (1995) Ph.D. Thesis, University of Munich, Germany.

Seewald, M.J., Pichumani, K., Stowell, C., Tibbals, B.V., Regan, L. and Stone, M.J. (2000) *Protein Sci.*, **9**, 1177–1193.

Suleiman, D. and Eckert, C.A. (1994) *J. Chem. Eng. Data*, **39**, 692–696.

Timasheff, S.N. (1992) *Biochemistry*, **31**, 9857–9864.

Timasheff, S.N. (2002) *Biochemistry*, **41**, 13473–13482.

Tjandra, N., Szabo, A. and Bax, A. (1996) *J. Am. Chem. Soc.*, **118**, 6986–6991.

Tollinger, M., Skrynnikov, N.R., Mulder, F.A., Forman-Kay, J.D. and Kay, L.E. (2001) *J. Am. Chem. Soc.*, **123**, 11341–11352.

van Nuland, N.A.J., Forge, V., Balbach, J. and Dobson, C.M. (1998) *Acc. Chem. Res.*, **31**, 773–780.

Vugmeyster, L., Kroenke, C.D., Picart, F., Palmer, III, A.G. and Raleigh, D.P. (2000) *J. Am. Chem. Soc.*, **122**, 5387–5388.

Wand, A.J., Ehrhardt, M.R. and Flynn, P.F. (1998) *Proc. Natl. Acad. Sci. USA*, **95**, 15299–15302.

Wilkins, D.K., Grimshaw, S.B., Receveur , V., Dobson, C.M., Jones, J.A. and Smith, L.J. (1999) *Biochemistry*, **38**, 16424–16431.